Chemical Science

ROYAL SOCIETY OF CHEMISTRY

EDGE ARTICLE

View Article Online
View Journal | View Issue

Cite this: *Chem. Sci.*, 2026, **17**, 1210

All publication charges for this article have been paid for by the Royal Society of Chemistry

Amyloidogenic oligomers derived from TDP-43 LCD promote the condensation and phosphorylation of TDP-43

Bryan Po-Wen Chen, †[ab] Chi-Chang Lee,†[a] Ruei-Yu He,[a] An-Chi Huang,[ab] Jie-rong Huang,[c] Jerry Chun Chung Chan *[b] and Joseph Jen-Tse Huang *[adefg]

The aberrant aggregation of TAR DNA-binding protein 43 (TDP-43) is a hallmark of amyotrophic lateral sclerosis (ALS). While TDP-43 aggregation can occur *via* both classical amyloidogenesis and phase separation-mediated mechanisms, the role of amyloidogenic oligomers in modulating TDP-43 condensation remains unclear. Herein, we employ a reverse micelle method to prepare uniform oligomers derived from the low-complexity domain of TDP-43, termed D1core oligomers. These amyloidogenic oligomers are toxic, potently induce phase separation of recombinant TDP-43 C-terminal domains, and promote phosphorylation of cytosolic TDP-43 condensates in cells. Compared to monomeric or fibrillar forms, D1core oligomers uniquely enhance the condensation propensity of wild-type TDP-43 and further potentiate aggregation of the ALS-associated A315T mutant. Live-cell studies using fluorescence recovery after photobleaching reveal that oligomer-induced condensates are modulated by HSP70, which preserves their liquid-like properties. These findings provide new insights into the interplay between TDP-43 oligomers, phase separation, and aggregation, advancing our understanding of ALS-related proteinopathy.

Received 21st July 2025
Accepted 13th November 2025

DOI: 10.1039/d5sc05433h

rsc.li/chemical-science

Introduction

TDP-43 has been linked to neurodegenerative diseases since its aggregates were found in the brains of patients with amyotrophic lateral sclerosis (ALS) and frontotemporal dementia (FTLD).[1] Subsequent studies revealed that these TDP-43 aggregates, which are hyperphosphorylated and ubiquitinated, are primarily composed of their low complexity domain (LCD) located in the C-terminal region.[2,3] Current studies have revealed that the LCD in TDP-43 is closely associated with its intermolecular self-assembly, autoregulation, and RNA splicing activity.[4,5] Nevertheless, it is worth noting that many LCDs are prone to misfolding, potentially leading to amyloid formation.[6–9] The aggregation of amyloidogenic proteins begins with a gradual primary nucleation phase, in which monomers assemble into oligomeric nuclei.[10,11] Subsequently, these nuclei (*e.g.*, oligomers) function as seeds to induce fibril formation by recruiting additional monomers. Increasing evidence suggests that the primary cytotoxic entities are soluble oligomers of TDP-43 LCD fragments rather than their fibrillar aggregates.[12,13] These oligomers reside within microvesicles or exosomes and can be transmitted between cell bodies (somata), inducing the formation of endogenous TDP-43 granules and subsequent toxicity in recipient cells.[14] Notably, in a mouse model, injecting oligomers derived from sonicated full-length TDP-43 fibrils into the motor cortex results in the propagation of pathological TDP-43 along pyramidal tract axons.[15] This phenomenon closely aligns with the progressive dissemination of pathology observed in motor neurons of ALS patients.

Beyond amyloidogenic aggregation, TDP-43 can undergo liquid–liquid phase separation (LLPS) in response to cellular stress, forming dynamic and membraneless organelles. This reversible process, mediated by interactions within its low-complexity domain (LCD), enables the formation of liquid-like condensates that support RNA transport and storage, particularly during stress adaptation.[16,17] Recent literature further suggests an interconnection between TDP-43 condensates and TDP-43 aggregates.[16,18,19] While LLPS is initially a reversible and functional process, prolonged or aberrant phase separation can

[a]*Institute of Chemistry, Academia Sinica, Taipei 115, Taiwan. E-mail: jthuang@gate.sinica.edu.tw*

[b]*Department of Chemistry, National Taiwan University, Taipei 106, Taiwan. E-mail: chanjcc@ntu.edu.tw*

[c]*Institute of Biochemistry and Molecular Biology, National Yang Ming Chiao Tung University, Taiwan*

[d]*Chemical Biology and Molecular Biophysics, Taiwan International Graduate Program, Academia Sinica, Taipei 115, Taiwan*

[e]*Department of Applied Chemistry, National Chiayi University, Chia-Yi 600, Taiwan*

[f]*Neuroscience Program of Academia Sinica, Academia Sinica, Taipei 115, Taiwan*

[g]*Sustainable Chemical Science and Technology, Taiwan International Graduate Program, Academia Sinica, Taipei 115, Taiwan*

† B. P. C. and C. C. L. contributed equally to this work.

drive the formation of solid-like aggregates, transitioning from liquid droplets to amyloid fibrils. This liquid-to-solid transition may serve as a mechanistic link between normal stress response and pathological aggregation. Moreover, emerging evidence suggests a potential connection between TDP-43 LLPS and oligomerization, wherein oligomeric species of the C-terminal domain (TDP-CTD, residues 266–414) exhibit biophysical similarities to TDP-CTD under LLPS conditions, as observed *via* electron paramagnetic resonance spectroscopy.[16] We surmise that oligomers may either exist within or actively promote LLPS. While LLPS is typically reversible and functional, it is thought that sustained or dysregulated phase separation can lead to the formation of stable aggregates.[20] This transition may represent a critical step in ALS pathogenesis, as liquid droplets lose fluidity and become pathological inclusions. To date, most pathological studies on TDP-43 have primarily focused on either the aging of cellular condensates or the role of oligomers in amyloidogenesis. However, the potential impact of these oligomers on TDP-43 condensation, as well as the resulting gelation and/or aggregation, remains largely unexplored.

Currently, it is known that the LLPS of TDP-43 is modulated by numerous factors, including molecular chaperones (like the heat shock protein 70kD, Hsp70), phosphorylation, and pathological mutations. Intriguingly, the role of HSP70 in modulating TDP-43 condensation and stress granules within cells remains debated. On one hand, HSP70 has been shown to stabilize TDP-43 in liquid-like condensates and prevent its transition into amyloid aggregates.[21] By contrast, within stress granules, which are transient cytosolic organelles formed through LLPS, HSP70 facilitates granule disassembly.[22] Given that TDP-43 condensation is closely associated with stress granule dynamics, understanding how these modulators influence TDP-43 behavior in response to oligomeric stimuli is of particular interest.

In this work, we aim to investigate how amyloidogenic fragments modulate the condensation of TDP-43 both *in vitro* and within cells. Previous studies have shown that proteolytic cleavage of TDP-43 in cells can generate amyloidogenic fragments that promote phosphorylation, a hallmark of TDP-43 proteinopathy, and accelerate monomer aggregation.[23] The protease-resistant core has been mapped to the LCD (residues 279–360), within which multiple amyloidogenic segments have been reported by our group and others.[24–26] In this study, we selected the defined amyloidogenic core previously identified by our group (D1core, residues 307–322) to characterize the direct interaction between amyloid fragments and TDP-43.[27] Using the reverse micelle (RM) method followed by counterionic extraction, we obtained well-defined oligomers of D1core. The physiochemical and amyloidogenic properties of these oligomers were characterized using various biophysical techniques. Furthermore, we examined the impact of D1core oligomers on the condensation propensity of the recombinant C-terminal domain of TDP-43 (residues 266–414). In cells, we further examined the condensation behavior of wild-type TDP-43 in response to D1core oligomers, focusing on its interplay with the stress granule marker, Ras-GTPase-activating protein SH3 domain-binding protein 1 (G3BP1) and the molecular chaperone HSP70. Notably, the ALS-linked mutant TDP-43 A315T exhibited a distinct condensation phenotype upon exposure to D1core oligomers, differing from the wild type in both G3BP1 colocalization and condensate fluidity.

Results and discussion

Preparation and characterization of oligomers from reverse micelles

To dissect the complex interplay between amyloidogenic oligomers and TDP-43 condensation, a robust and reproducible method for generating uniform, high-quality oligomers is essential. To this end, we employed RMs to prepare the oligomers of a TDP-43 fragment.[28,29] Amyloidogenic peptides derived from the C-terminus of TDP-43, including the D1core and its fluorophore-tagged counterpart (TAMRA-D1core; see Table S1 for the structure), were synthesized using microwave-assisted solid-phase peptide synthesis. The peptides were purified by high-performance liquid chromatography and verified by mass spectrometry (details in the SI). D1core oligomers were prepared in RMs formed by introducing the negatively charged surfactant dioctylsulfosuccinate sodium salt (AOT) into isooctane. Monomeric D1core peptides in Tris buffer were then added to the RM solution. The hydrophilic core of the RMs, with $W_0 = 70$ (molar ratio of water to surfactant), was found to be tens of nanometers in diameter (*vide infra*). Through dynamic fusion and fission of RMs, the encapsulated peptides oligomerized within the constrained micellar volume.

To back-extract the D1core oligomers from the RM solution (incubated for at least 7 days in the RMs), we added tri-*n*-octylmethyl-ammonium chloride (TOMAC), a cationic surfactant in water, to co-precipitate residual AOT in the organic phase (Fig. 1a). We found that the addition of TOMAC significantly enhanced the extraction efficiency of the oligomers. To quantify this efficiency, we prepared oligomers of TAMRA-tagged D1core (TAMRA-D1core) in RMs. The extraction yield was then estimated by measuring the relative absorbance of TAMRA ($\lambda_{max} = 560$ nm) in both the organic and aqueous phases (Fig. S1). With TOMAC, we achieved complete extraction of the oligomers into the aqueous phase, whereas without TOMAC, the yield was only approximately 20%. The extracted oligomers in the aqueous phase were subsequently collected by lyophilization for further experiments (details in the SI).

For the following characterization studies, different states of D1core peptides were examined, with the corresponding preparation protocols described in the Materials and methods section ("Preparation of D1core peptides in different states"). TEM images were acquired for the extracted D1core oligomers. D1core freshly prepared from RMs showed abundant oligomers under a transmission electron microscope, with diameters around 25–40 nm (Fig. 1b). By contrast, directly incubated D1core monomers, without prior treatment in reverse micelles, did not yield detectable oligomeric aggregates (Fig. S2a). After 4–7 days of incubation, further fibrillization was observed in both back-extracted and directly incubated samples (Fig. 1c, d and S2b, c). In parallel, dynamic light scattering (DLS) revealed that the hydrodynamic size of oligomers was

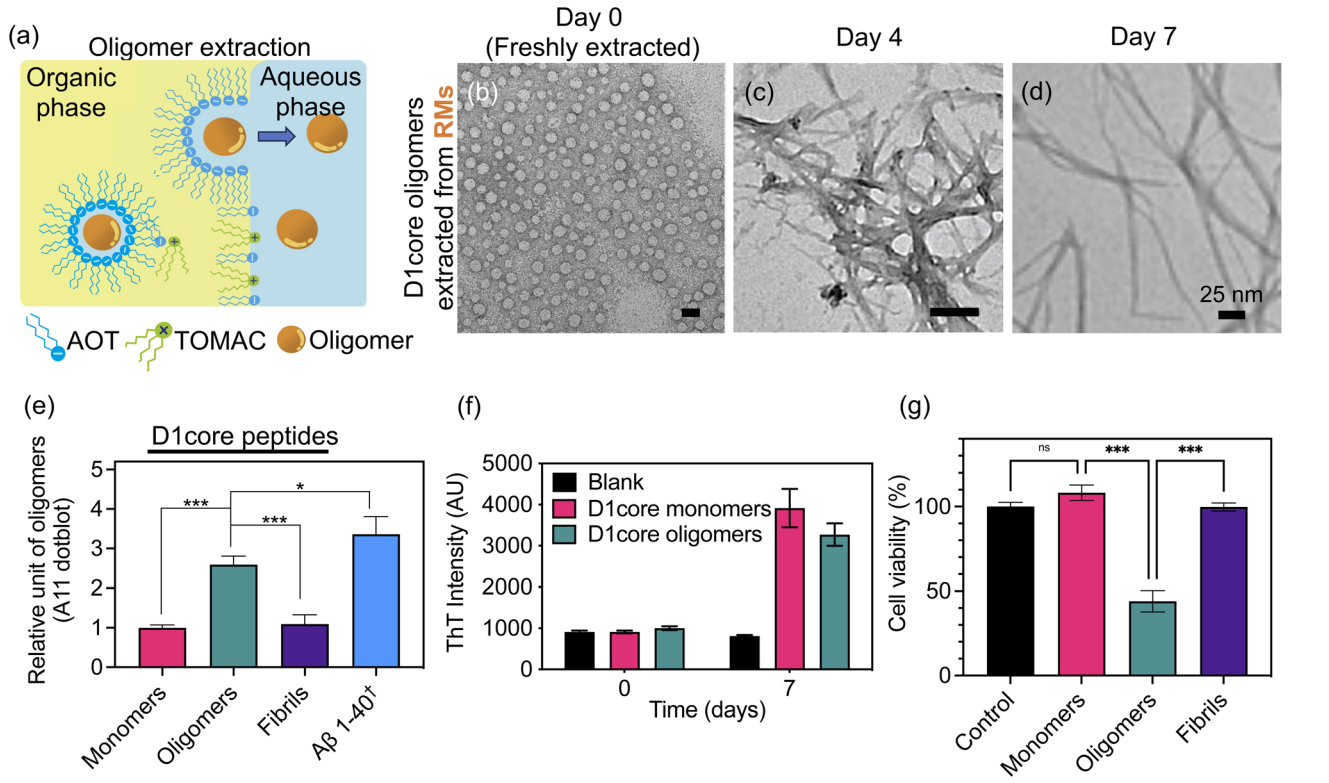

Fig. 1 Characterization of D1core oligomers after back-extraction from the RMs. (a) Schematic illustration of the back-extraction process of oligomers *via* the addition of a counterionic surfactant. (b–d) TEM images of freshly back-extracted D1core oligomers (b) and after further incubation for 4 days (c) and 7 days (d). (e) A11 dot blotting analysis of D1core in monomeric, oligomeric, and fibrillar states. †$A\beta_{40}$ peptide, incubated for 2 hours at 25 °C. (f) Fluorescence intensity of ThT (200 μM) in the presence of monomeric or oligomeric D1core peptides (50 μM). (g) The alamarBlue assay of U2OS cells treated with D1core peptides (2.5 μM) for 18 hours. Data were analyzed by one-way ANOVA using Tukey's post-hoc test with 95% confidence interval, with $*p$ <0.05, $**p$ <0.01, and $***p$ <0.001. The statistical results are shown as mean ± SD of 3 independent replicates.

approximately 66 nm (Fig. S3a), consistent with the size observed by TEM. Moreover, both monomers and oligomers showed negligible turbidity, indicating the absence of large particles, whereas fibrils exhibited noticeable turbidity (Fig. S3b). These results suggest that D1core in RMs underwent oligomerization through RM fusion and fission. Upon removal of the RM constraint, the oligomers proceeded to further fibrillization. Compared to the extracted D1core, in which oligomers were enriched (Fig. 1b), directly incubated D1core resulted in heterogeneous species (*i.e.*, oligomeric and fibrillar; Fig. S2b).

To further assess whether the oligomers extracted from RMs retained their amyloidogenic nature, we examined their secondary structure using circular dichroism (CD). The spectrum revealed that the oligomers were predominantly random coil, whereas fibrillization resulted in a clear β-sheet signature characterized by a negative peak around 220 nm (Fig. S3c). Furthermore, the oligomer-specific antibody A11 was applied in a dot blot assay. A concentration of 50 μM $A\beta_{40}$ peptide, incubated for 2 hours at 25 °C, served as a positive control for the A11 assay. We found that the oligomers freshly extracted from RMs were recognized by the A11 antibody, whereas D1core monomers and fibrils showed weaker signals (Fig. 1e). Furthermore, we used the thioflavin T (ThT) assay to monitor amyloid fibril formation during oligomer incubation. After 7 days, the D1core oligomers exhibited increased ThT fluorescence, comparable to that observed for monomeric D1core peptides (Fig. 1f). Finally, the toxicity of D1core peptides was evaluated by the alamarBlue assay in U2OS cells. At 2.5 μM, both monomers and fibrils exhibited no significant toxicity, whereas D1core oligomers extracted from RMs reduced cell viability by approximately 44% (Fig. 1g). The residual AOT concentration in these experiments was estimated to be ~42 μM (peptide : AOT molar ratio = 1 : 16.8) by NMR measurements (Fig. S4), a level that showed negligible toxicity (Fig. S5).

Through these experiments, we confirmed both the feasibility and stability of the RM method for preparing D1core oligomers. We further evaluated the shelf life of RMs containing D1core oligomers. DLS analysis showed that the RMs maintained a consistent particle size of 35–40 nm for up to 90 days (Fig. S6a). Moreover, ThT kinetic measurements indicated that oligomers extracted from RMs after at least four days of incubation exhibited consistent fibrillization behavior, with samples incubated for 4–90 days showing similar kinetics (Fig. S6b). Collectively, these findings validate the RM approach as a robust and shelf-stable method for producing amyloidogenic oligomers suitable for downstream applications.

D1core oligomers promoted the condensation of recombinant TDP-CTD

Nanoscale protein assemblies have been reported to act as precursors that promote the LLPS of proteins containing low-complexity domains (LCDs).[30] Inspired by this finding, we hypothesized that protein LLPS could be driven by a clustered core that engages in multivalent interactions with the LCDs of surrounding proteins, thereby recruiting soluble proteins and facilitating their phase separation in a manner reminiscent of protein seeding. In a cell-free TDP-43 expression system, we observed that D1core oligomers, but not monomers or fibrils, robustly induced TDP-43 aggregation (Fig. S7), suggesting that oligomeric assemblies mediate a specific interaction with TDP-43. These findings prompted us to investigate whether D1core oligomers can directly promote TDP-43 condensation.

To examine this, we employed recombinant TDP-CTD (residues 266–414), a C-terminal fragment of TDP-43 encompassing the LCD and known to undergo LLPS.[31,32] To trace the localization of D1core peptides, each form of peptide solution (monomeric, oligomeric, and fibrillar) was spiked with 10% TAMRA-labelled D1core. Differential interference contrast (DIC) microscopy revealed that TDP-CTD formed spherical puncta, which completely dissolved upon incubation with 1,6-hexanediol (1,6-HD), confirming the fluidic nature of the TDP-CTD condensates (Fig. 2a and b; inset shows a zoomed-in condensate), as 1,6-HD selectively dissolves condensates but not aggregates.[33] Upon the addition of different forms of D1core peptides, we found that D1core oligomers significantly colocalized with and promoted TDP-CTD condensation (Fig. 2e), as indicated by increases in both the condensate number (Fig. 2i) and size (Fig. 2j). By contrast, although the monomeric and fibrillar forms of D1core also colocalized with TDP-CTD condensates (Fig. 2c and g), they failed to promote condensation (Fig. 2i and j). Furthermore, the fluidic properties of the TDP-CTD condensates were maintained in the presence of all forms of D1core peptides, as evidenced by their dissolution with 1,6-HD (Fig. 2d, f and h). Notably, under TDP-CTD and fibrillar D1core containing conditions, a trace amount of aggregates

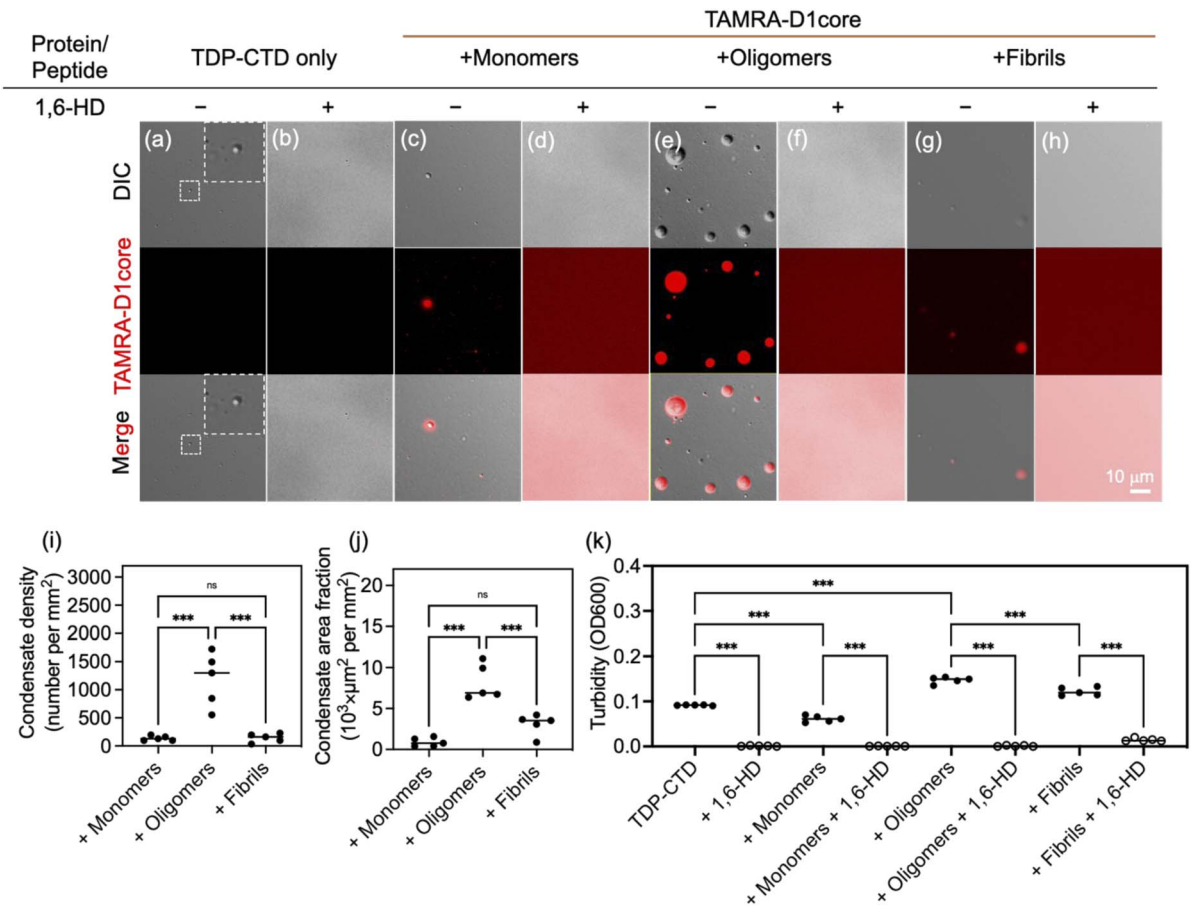

Fig. 2 Characterization of TDP-CTD condensates in the presence of D1core peptides. (a–h) DIC and fluorescence microscopy images of TDP-CTD (25 μM) with different D1core peptide states: (a) TDP-CTD alone, (c) with monomeric D1core peptides, (e) with oligomeric D1core peptides, and (g) with fibrillar D1core peptides, all without 1,6-HD (22.5 μM D1core and spiked with 2.5 μM TAMRA-D1core). Panel (a), the dashed square indicates the region shown in the zoom-in inset image. Panels (b), (d), (f), and (h) show the same samples in the presence of 20% 1,6-HD. (i and j) Condensate density (i) and total condensate area (j) were quantified using ImageJ based on the fluorescence channel of TAMRA. (k) Optical density at 600 nm (OD_{600}) of TDP-CTD alone and with D1core peptides, without and with 20% 1,6-hexanediol. Data were analyzed by one-way ANOVA using Tukey's post-hoc test with 95% confidence interval, with *p <0.05, **p <0.01, and ***p <0.001. The statistical results are shown as mean ± SD of 5 independent replicates.

remained even after 1,6-HD treatment, which may be due to residual D1core fibrils or aggregates (Fig. S8).

To further evaluate the extent of condensate formation, we measured solution turbidity at 600 nm (OD_{600}) using D1core peptides without TAMRA labelling. Among the three forms tested, only D1core oligomers significantly increased the turbidity of the TDP-CTD solution, whereas the monomeric and fibrillar D1core had minimal effects (Fig. 2k). Upon treatment with 1,6-hexanediol (1,6-HD), the turbidity decreased to nearly zero, consistent with the dissolution of condensates. A small residual turbidity signal was observed under fibril-containing conditions, likely due to the presence of pre-formed D1core fibrils, as noted earlier (Fig. S8).

Collectively, our findings demonstrated that D1core oligomers can promote the condensation of TDP-CTD. We speculate that this phenomenon may arise from the interactions between the LCDs of D1core oligomers and TDP-CTD. Next, we explored whether this condensation-promoting effect is also conserved with full-length TDP-43 in the mammalian cellular context.

D1core oligomers induced the cytosolic condensation of wild-type TDP-43, and its fluidity was maintained by HSP70

With this in mind, we investigated the impact of D1core peptides on cytosolic TDP-43 condensation, with particular focus on their influence on condensation propensity and fluidity dynamics of the resulting condensates, as schematized in Fig. 3a. Using the TAMRA-labelled D1core, we confirmed that the peptides successfully penetrated cells and localized within the cytosol, as demonstrated by fluorescence microscopy (Fig. 3b–d). Next, to visualize how TDP-43 responds to oligomers, the cells were transfected with wild-type eGFP-TDP-43 prior to D1core treatment. We hypothesized that treatment with D1core oligomers would promote LLPS and induce the formation of TDP-43 condensates in cells. Indeed, in cells expressing eGFP-TDP-43, the introduction of D1core oligomers led to the formation of cytosolic TDP-43 condensates, a phenomenon significantly more pronounced compared to cells treated with monomeric or fibrillar D1core (Fig. 3e–h; low-magnification micrograph images in Fig. S9). We further investigated the relationship between TDP-43 condensates and endogenous G3BP1, given the potential involvement of stress granules in ALS/FTLD pathology.[20,34,35] Immunostaining with a G3BP1 antibody (Fig. 3e–g) revealed that co-localization of TDP-43 condensates with G3BP1 following treatment with D1core oligomers (Fig. 3f and i), suggesting that these TDP-43 condensates were components of stress granules. Additionally, we found that the TDP-43 within the condensates was phosphorylated, as shown by immunostaining (anti-pS409/410; Fig. 3f and i), further indicating their relevance to proteinopathy. To assess the fluidity of these cellular condensates, we performed fluorescence recovery after the photobleaching (FRAP) assay with cells co-expressing mCherry-G3BP1 and eGFP-TDP-43, as aging and the loss of fluidity in condensates are thought to contribute to pathology.[36] Interestingly, both TDP-43 and G3BP1 remained fluidic within the condensates even after 18 hours of treatment (Fig. 3j).

In TDP-43 condensates, it is generally believed that many cellular protein compartments help maintain condensate fluidity. Among them, heat shock proteins (HSPs) have been implicated in facilitating condensate disassembly and preventing gelation or aggregation.[36,37] *In vitro* studies further suggest that HSP70 can inhibit the gelation or aggregation of LCD-containing proteins such as FUS and TDP-43.[21,38] Based on this, we hypothesized that HSP70 may help preserve the fluidity of eGFP-TDP-43 condensates promoted by D1core oligomers. Immunostaining with a specific antibody against HSP70 on D1core oligomer-treated cells overexpressing eGFP-TDP-43 revealed that HSP70 was colocalized with cytosolic eGFP-TDP-43 condensates (Fig. S10). We included the HSP70 inhibitor (HSPi), VER-155008, in our cell experiments to learn its functional role in maintaining condensate fluidity. Cells treated with HSPi, oligomers, or both exhibited cytosolic eGFP-TDP-43 condensates that colocalized with G3BP1 (Fig. 3k–m); fluorescence profiles are shown in Fig. S11; a quantitative analysis of cells with cytosolic eGFP-TDP-43 condensates treated with HSPi, D1core oligomers, or both is included as Fig. S12.

As shown in Fig. 3n and o, cells treated with either HSPi (green curves) or oligomers alone (red curves) displayed relatively high fluorescence recovery, indicating that the condensates remained fluidic. In contrast, when both HSPi and oligomers were applied, fluorescence recovery was significantly reduced (blue curves), suggesting a transition toward a gelled or aggregated state. Together, these results indicate that HSP70 maintains the fluidity of cytosolic TDP-43 condensates by counteracting D1core oligomer-induced gelation.

D1core oligomers induced the aggregation/gelation of pathological TDP-43 mutant (A315T) condensates

In addition to examining wild-type TDP-43, for which HSP70 helps maintain condensate fluidity, we also investigated the condensation behaviour of the ALS-associated A315T mutant of TDP-43.[39,40] This mutation is known to enhance aggregation propensity, and we anticipated that its condensates might behave differently from those of the wild-type protein. Similar to wild-type TDP-43, treatment with D1core oligomers induced pronounced cytosolic condensation of eGFP-A315T along with phosphorylation (Fig. 4a–e; low-magnification images are shown in Fig. S13). However, unlike wild-type TDP-43 condensates, which largely colocalized with G3BP1 in the presence of oligomers (Fig. 3f), the eGFP-A315T condensates were juxtaposed to G3BP1 (Fig. 4b and e). Furthermore, in the FRAP assay, eGFP-A315T condensates exhibited relatively low recovery, hinting at a transition toward gelation or aggregation in contrast to the mCherry-G3BP1 signal, which remained highly dynamic (Fig. 4f). In addition, HSP70 was still detected within cytosolic condensates (Fig. S10). However, the presence of HSP70 seemed insufficient to preserve the fluidity of A315T condensates (Fig. 4f).

Despite the differing physical behaviour of G3BP1 and TDP-43, both wild-type and A315T variants showed cytosolic accumulation of phosphorylated TDP-43 following D1core oligomer treatment (Fig. 3f and 4b). These observations suggest that the oligomer-induced condensation of TDP-43, in both cases, may be

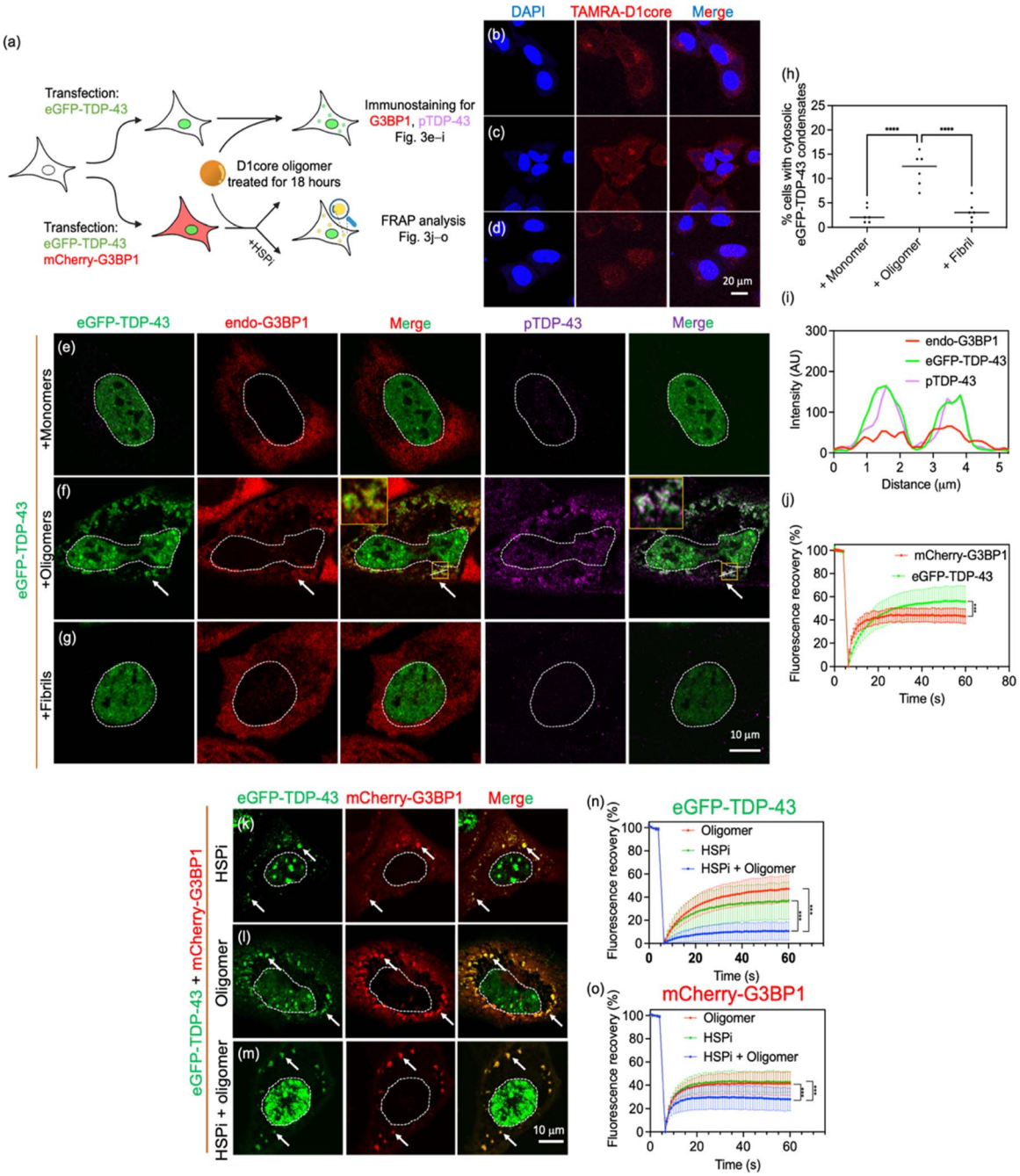

Fig. 3 D1core oligomers induced cytosolic TDP-43 condensation. (a) Schematic illustration of experimental design to assess the impacts of D1core peptides on cytosolic TDP-43 condensation. (b–d) Confocal images of U2OS cells treated with 2.5 μM TAMRA-D1core for 18 hours. (e–g) Fluorescence images of U2OS cells transfected with eGFP-TDP-43 followed by immunostaining of endogenous G3BP1 and phosphorylated TDP-43 (condensates are arrowed) in the presence of monomeric (e), oligomeric (f) and fibrillar (g) D1core peptides, respectively. (h) Quantification of cells with cytosolic eGFP-TDP-43 condensates in the presence of D1core peptides. Data were analysed by one-way ANOVA using Tukey's post-hoc test with 95% confidence interval, with $*p$ <0.05, $**p$ <0.01, and $***p$ <0.001. Results are presented as mean ± SD from five independent replicates, with 150 cells counted per replicate. (i) Fluorescence profiling of eGFP-TDP-43, endo-G3BP1, and phosphorylated TDP-43 in the presence of D1core oligomer along the cross section indicated in (f). (j) FRAP analysis of cytosolic condensates in cells co-expressing mCherry-G3BP1 and eGFP-TDP-43 following treatment with D1core oligomers to assess condensate fluidity. FRAP data are presented as mean ± SD (n ≥20) of fluorescence recovery (%) at 60 s. Data were analysed by two-way ANOVA using Tukey's post-hoc test with 95% confidence interval, with $***p$ <0.001. (k–m) Fluorescence images of cells co-expressing mCherry-G3BP1 and eGFP-TDP-43 treated with D1core oligomers, HSPi, or both. (n and o) FRAP analysis of cytosolic eGFP-TDP-43 (n) and mCherry-G3BP1 (o) condensates after 18 hours of D1core oligomer treatment. Statistical results of FRAP analyses are shown as mean ± SD (n ≥20) of fluorescence recovery (%) at 60 s post-bleaching. Data were analysed by two-way ANOVA using Tukey's post-hoc test with 95% confidence interval, with $***p$ <0.001.

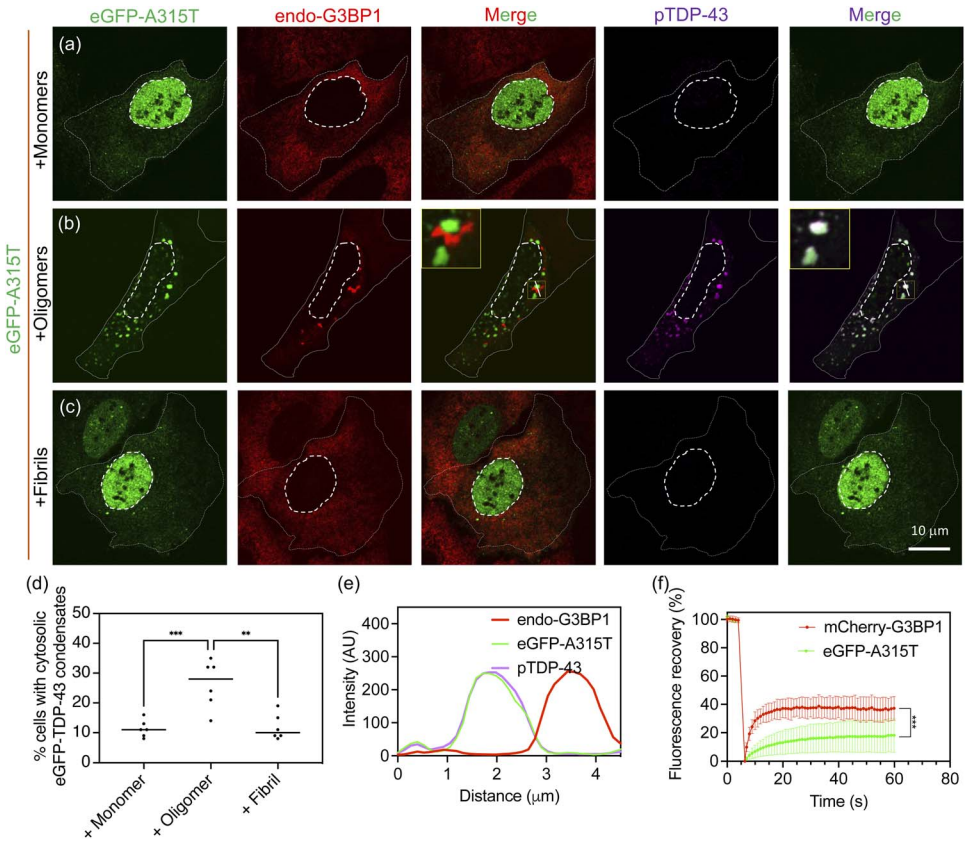

Fig. 4 D1core oligomers induced cytosolic A315T condensation. (a–c) Fluorescence images of U2OS cells transfected with eGFP-A315T followed by immunostaining of endogenous G3BP1 and phosphorylated TDP-43 (condensates are arrowed) in the presence of monomeric (a), oligomeric (b) and fibrillar (c) D1core peptides, respectively. (d) Quantification of cells with cytosolic eGFP-A315T condensates in the presence of D1core peptides. Data were analyzed by one-way ANOVA using Tukey's post-hoc test with 95% confidence interval, with *p <0.05, **p <0.01, and ***p <0.001. Results are presented as mean ± SD from five independent replicates, with 150 cells counted per replicate. (e) Fluorescence profiling of eGFP-A315T, endo-G3BP1 and phosphorylated TDP-43 in the presence of D1core oligomer with the cross section indicated in (b). (f) FRAP analysis of condensates in cells co-expressing mCherry-G3BP1 and eGFP-A315T after D1core oligomer treatment to assess fluidity. Statistical results of FRAP analyses are shown as mean ± SD (n = 22) of fluorescence recovery (%) at 60 s post-bleaching. Data were analyzed by two-way ANOVA using Tukey's post-hoc test with 95% confidence interval, with ***p <0.001.

relevant to ALS/FTLD pathology.[1] Based on these findings, we concluded that D1core oligomers can induce cytosolic condensation of both wild-type and A315T TDP-43, while the A315T mutant shows further inclination to gelation or aggregation.

In this study, we demonstrated the specific recruitment of HSP70 to TDP-43 condensates upon exposure to D1core oligomers (Fig. S10). While HSP70 may also interact with D1core oligomers, several lines of evidence support a primary engagement between HSP70 and TDP-43 condensates. Under cellular stress conditions (*e.g.*, heat shock or oxidative stress), HSP70 colocalizes with TDP-43 foci, consistent with a chaperone–client interaction.[21,41,42] Moreover, mapping studies have identified a conserved HSP70-interaction hotspot within the TDP-43 LCD (residues 320–340),[21] which minimally overlaps with the D1core fragment (residues 307–322). Given that HSP70 typically recognizes short, solvent-exposed motifs in disordered clients, these findings suggest that HSP70 preferentially engages TDP-43 within condensates.

Amyloidogenic oligomers have long been recognized as important dynamic entities in neurodegenerative diseases.[11] These oligomers exist in various states characterized by differences in size, conformation, and cellular responses, posing challenges for pathology studies and drug development.[43] Therefore, acquiring uniform oligomers with a predetermined state is critical. Taking advantage of RMs, different states of oligomers could be obtained by manipulating the size of RMs through adjustments in their water-to-surfactant ratio.[44] Moreover, the notable stability of oligomers within RMs ensures rigorous quality control, a crucial aspect that could significantly benefit our understanding toward the structural details of oligomers. For instance, RMs have been applied to study the structures of Aβ oligomers, highlighting their potential as a powerful tool in amyloid research.[28,44,45]

To date, the precise molecular structures of amyloidogenic oligomers remain unresolved. However, several techniques have indicated the presence of substantial β-sheet strands in these oligomers.[44,46,47] During protein assembly, it is possible that the β-strands within D1core oligomers act as templates for intermolecular interactions with TDP-43, facilitating the recruitment of soluble TDP-43 *via* its LCD undergoing condensation. This interaction is supported by the seeding experiments (Fig. S7), where D1core oligomers interacted with

TDP-43 LCDs, ultimately leading to their aggregation. Previously, our group identified a scrambled sequence of D1core (ScD1core) that, despite being amyloidogenic, failed to seed the TDP-43 protein like the original D1core peptide.[27] This result suggested that seeding requires sequence-specific interactions with TDP-43. Consistently, we found that ScD1core oligomers prepared in reverse micelles also failed to promote TDP-CTD condensation (Fig. S14). Together, we inferred that similar interactions may underlie the promotion of TDP-43 condensation.

The aging of TDP-43 condensates is thought to play a role in ALS/FTLD pathology.[18,20,48,49] To study cellular TDP-43 condensation, stressors such as arsenite or sorbitol[18,35] along with genetic mutations (*e.g.*, deletion of the nuclear localization signal, ΔNLS)[18] have frequently been applied to recapitulate ALS-like phenotypes, including TDP-43 condensation and mislocalization, in cells.[18,20,49] However, these reagents may also trigger unrelated non-specific cellular stress responses.[50] In this study, we instead utilized disease-relevant D1core oligomers to elicit TDP-43 condensation, allowing a more disease-relevant comparison.

Accordingly, we showed that D1core oligomers can trigger cytosolic condensation of wild-type TDP-43 and promote aggregation of its A315T variant. In wild-type TDP-43, the induced condensates colocalized with G3BP1 and remained dynamic, suggesting a stress granule-like property. These structures were phosphorylated and required HSP70 activity to maintain fluidity, implying that phosphorylation and chaperone function acted together to preserve a reversible, regulated state. This supports the idea that phospho-TDP-43 may mark an early, protective phase of condensation rather than a terminal aggregation state.[51] In contrast, A315T forms more rigid, G3BP1-negative condensates, indicating a direct phase transition toward aggregation. Together, these findings suggest that early TDP-43 condensation is tuneable and regulated and that phosphorylation might serve to delay its pathological transition.

Conclusion

This work establishes a reliable and effective protocol for stabilizing homogeneous D1core oligomers in RMs with satisfactory shelf life. The back-extracted D1core oligomers were found to promote the condensation of recombinant TDP-CTD. Notably, upon oligomer treatment, wild-type TDP-43 formed condensates that remained dynamic and chaperone-responsive, while the A315T mutation promoted a shift toward less reversible and aggregated assemblies. Oligomer-induced TDP-43 cytosolic condensation may serve as a mechanistic bridge between reversible phase separation and irreversible aggregation, potentially contributing to neurodegenerative pathology.

Materials and methods

Peptide synthesis

The peptides were synthesized on rink amide AM resin using a peptide synthesizer (CEM, USA). The peptides were cleaved from the resin by using a cocktail of 94 : 2.5 : 2.5 : 1 TFA/H_2O/EDT/TIS, which were reacted for 3 hours and then precipitated in ice-cold MTBE. Finally, the peptides were purified by HPLC (Agilent, USA) on a C18 column (Shiseido, Japan) using a gradient of water/acetonitrile with 0.1% TFA. The molecular masses of the purified peptides were confirmed by matrix-assisted laser desorption ionization (MALDI) mass spectrometry. For fluorescence imaging, peptides were labelled with 5(6)-carboxytetramethylrhodamine, succinimidyl ester (TAMRA-SE). First, ~30 μg peptides were dissolved in 100 μL DMSO with 10 μL triethylamine. Then, 20 μL of TAMRA dye (1 mM) was added into the peptide solution and reacted for 1 hour at 30 °C with shaking. The crude product was finally purified by HPLC. The molar extinction coefficient of the TAMRA labelled peptide was about 65 000 M^{-1} cm^{-1}, as estimated using UV-vis spectrometry.

Preparation and incubation of peptide monomers

The purified peptides (~2 mg) were first pretreated with HFIP and sonicated in an ice bath for 1.5 hours. HFIP was then removed by drying under a nitrogen stream, followed by 2 hours of lyophilization. The resulting peptide powders were rehydrated with 1 mL Tris buffer (20 mM, pH 7.4). The samples were sonicated for 5 minutes and ultracentrifuged at 220 000*g* at 4 °C for 1 hour. The supernatant (90% of the volume from the top) was carefully collected and quantified by UV-vis spectrometry. It is important to note that the absorbance spectrum of D1core′s phenylalanines should show three distinct vibronic bands centered at 254 nm. If the spectrum displays a continuous band extending to around 340 nm, the peptide either requires re-treatment with HFIP or should be discarded. The final peptide concentrations were diluted to 50 or 150 μM with 20 mM Tris buffer (pH 7.4) for subsequent experiments.

Formation of oligomers in reverse micelles

The reverse micelle preparation process was adapted from a previously reported method.[28,29] First, a solution of 132.1 mM AOT (dioctyl sulfosuccinate sodium salt) in isooctane was prepared. To 3 mL AOT isooctane solution, 0.5 mL of freshly prepared peptide solution (150 μM) was added [W_0(water loading) = 70]. The resultant solution was sonicated for 5 minutes and stored at 25 °C under quiescent conditions for 7–90 days before the extraction, as the storage time in RMs showed consistent aggregation kinetics in the ThT assay. The extraction process of peptide oligomers from the reverse micelles is as follows. A 5% (w/w) aqueous suspension of methyltrioctylammonium chloride (TOMAC) was prepared and sonicated in a water bath for 10 min before each use (the solution appears turbid and white). To extract the peptides, the solutions of reverse micelles in isooctane and TOMAC in water were mixed with equal volumes and shaken with a turbo mixer at 3000 rpm for 2 min. The emulsion was then centrifuged at 12 200*g* at 4 °C for 1 hour. The aqueous phase of the solution containing 20 μM D1core was collected and lyophilized. The powder was rehydrated with water to a final peptide concentration of 50 μM for incubation. The rehydrated peptide

solution should be completely clear after few times of pipetting. While collecting the aqueous parts, the organic phase was first removed using a pipette, then 90% vol. of the solution was collected with microloader tips or long pipette tips. The protocol was to avoid wrongly collecting the organic part of the solution. The lyophilized powder should not be kept in the refrigerator or lyophilizer for longer than 24 hours.

Dot blot assay

Two aliquots of peptide solutions (2.0 μL for each) were applied to a nitrocellulose membrane (GE Healthcare, USA) of 0.1 μm pore size. The membrane was immersed in blocking buffer (2% BSA in TBS-T) for 30 min with gentle shaking. The oligomer antibody, A11 (Sigma-Aldrich, USA), diluted with a blocking buffer (1 : 5000) was then applied overnight with shaking. The membrane was washed with TBS-T three times (10 min with shaking each time). Finally, the membrane was transferred to the solution of secondary antibody [HRP-conjugated antirabbit antibody in blocking buffer (1 : 5000)] for 45 min of staining and again washed three times with TBS-T. The HRP complexes on membrane were detected on a Biospectrum® AC image system (UVP, USA) using a chemiluminescent substrate for HRP (Millipore, USA). The blotting signals were analyzed with ImageJ (National Institutes of Health, Bethesda, MD).

Transmission electron microscopy (TEM)

An aliquot (10 μL) of sample was suspended on a glow-discharged carbon-coated copper grid for 1 min and dried. The grid was washed with water drip 2 times and stained with 2% uranyl acetate for 30 s. The grid was dried in a high vacuum overnight at 25 °C before submission to TEM analysis. TEM images were recorded with a FEI Tecnai G2 TF20 TWIN electron microscope operated at 120 kV.

Dynamic light scattering (DLS)

An aliquot (800 μL) of sample (20 μM) in Tris buffer was placed in a 1.0 cm plastic cuvette and measured at 25 °C using a Zetasizer Lab (Malvern Panalytical).

Circular dichroism spectroscopy (CD)

An aliquot (250 μL) of sample (25 μM) in Tris buffer was placed in a 0.1 cm quartz cuvette and measured at 20 °C using a J-815 spectrometer (JASCO, Japan).

Thioflavin T (ThT) binding assay

Experiments were performed using a PerkinElmer ELISA microplate reader. One aliquot of peptide solution (50 μM) in Tris buffer was mixed with the same volume of ThT (200 μM). The ThT fluorescence emission spectra were recorded from 462 to 600 nm (EX = 442 nm).

Preparation of D1core peptides in different states

The monomeric state peptides were prepared by mixing freshly prepared D1core monomers with a stoichiometric amount of AOT (1.0 μM peptides corresponding to 16.7 μM AOT in buffer). The D1core oligomers were freshly extracted from the reverse micelles as mentioned above. The D1core fibrils were prepared from incubation of D1core oligomers longer than 14 days at 37 °C.

Purification of the TDP-CTD protein

Purification of TDP-CTD was performed following a previously published protocol.[31,32,52] In short, the construct of the C-terminal domain of TDP-43 (residues 266–414) containing a hexahistidine tag was expressed and isolated from inclusion bodies using 8 M urea. The extracted protein was initially purified using nickel-charged immobilized metal-ion affinity chromatography (IMAC; QIAGEN) followed by further purification on a C4 reverse-phase column (Thermo Scientific) *via* HPLC. The eluted protein was lyophilized for 24 h, subsequently incubated with 1,1,1,3,3,3-hexafluoro-2-propanol (HFIP) at a concentration of 1 mg mL^{-1} for 24 h at room temperature to disrupt potential aggregates and finally lyophilized again for 24 h. Lyophilized samples were stored in a dry cabinet.

Differential interference contrast (DIC) microscopy and turbidity experiments of TDP-CTD condensates

The concentration of TDP-CTD was determined by measuring the absorbance at 280 nm. TDP-CTD and D1core peptides (spiked with 2.5 μM TAMRA-D1core) were mixed to a final concentration of 25 μM each in a buffer containing 40 mM phosphate, 10 mM Tris and 100 mM NaCl (pH 7.2). For samples containing TDP-CTD alone, 418.0 μM AOT was presented in the same buffer to match the residual surfactant present during the D1core preparation. To dissolve the TDP-CTD condensate, 20% of 1,6-hexanediol (1,6-HD) was presented in the solution, and the mixture was shaken at 1400 rpm for 20 min. Differential interference contrast (DIC) images were captured using a 64× oil immersion objective on a Nikon Tie microscope. Turbidity (OD_{600}) was measured using a JASCO J-815 spectrometer at 25 °C. Quantitative analysis of TDP-43 condensates was conducted using ImageJ, where threshold functions were applied to the fluorescence channel (TAMRA) to analyze and quantify the area and number of droplets. Irregular aggregates in the fibril sample were manually excluded during the quantification process.

Cell free system and seeding experiments

The eukaryotic cell-free system derived from the rabbit reticulocyte lysate (TNT T7 Quick-Coupled Transcription/Translation System, Promega, USA) was applied to generate TDP-43 protein. 10 μL TNT master mix, 0.25 μL methionine (1 mM) and 0.5 μL plasmid (FLAG-TDP-His) were incubated at 30 °C for 4 h for protein synthesis. Later, 4.5 μL seed solutions were added into cell-free cocktails for further reaction at 30 °C for 20 h. To evaluate the seeding abilities of seeds, the samples were divided into supernatant and pellet fractions by centrifugation at 16 100*g* for 30 minutes at 4 °C. The pellet was then dissolved in SDS-PAGE loading buffer (50 mM Tris–HCl, pH 6.8, 7.5% glycerol, 1% SDS, 0.02% bromophenol blue and 1% β-mercaptoethanol), and the proteins in the supernatant were precipitated

with acetone for 18 hours followed by resuspension with the SDS-PAGE loading buffer. TDP-43 in both fractions was detected by western blotting with the primary anti-FLAG M2 monoclonal antibody (Sigma, USA). The antibody–TDP-43 complexes were detected with a BioSpectrum®AC imaging system (UVP, USA) using a chemiluminescent HRP substrate (Millipore, USA). The blotting signals were analyzed using ImageJ, and the fraction of TDP-43 protein in the supernatant was determined using the equation $S/(S+P)$, where S and P denote the signals of TDP-43 in supernatant and pellet fractions, respectively. All the experiments for each sample were repeated three times.

Cell viability

U2OS cells were purchased from ATCC (HTB-96) and were cultured at 37 °C and 5% CO_2 in McCoy's 5A (modified) medium (Gibco) supplemented with 10% (vol/vol) fetal bovine serum (FBS) and 100 U per mL penicillin–streptomycin. For viability experiments, the cells were inoculated in a 96-well plate. After 24 h of incubation, the culture medium was replaced by 200 μL of peptide-containing medium, and the cells were incubated for another 18 h. The peptides (2.5 μM) in different states (monomeric, oligomeric and fibrillar D1core) were lyophilized and rehydrated with medium before the cell treatments. The cell viability was determined using the alamarBlue assay by detecting the absorbance at 570 nm. The cell viability ratio was calculated as: viability = (sample − background)/(ctrl − background) × 100%. The error bars indicated SEM from the means of three independent experiments.

Cell culture and transfection

Plasmids were transfected into U2OS cells using Lipofectamine 3000 reagent in Opti-MEM with the plasmid (0.5 μg) to P3000 (μL) to Lipofectamine 3000 (μL) ratio of 1 : 1 : 1. eGFP-TDP-43-WT was provided by Dr Pang-Hsien Tu. eGFP-TDP-43-A315T was created with site-directed mutagenesis (primer sequences: F′: gaactttggtacgttcagcattaatc; R′: gattaatgctgaacgtaccaaagttc). mCherry-G3BP1 was created with In-Fusion Snap Assembly cloning kits (Takara Bio, Shiga, Japan) and cloned into an in-house C-terminally fused mCherry vector. Primer sequences: Frag1_F′: ttcgaattctgcagtcgacgatggtgatggagaagcctagt; Frag1_R′: tatgtctgcaggtgctggagaagaactct; Frag2_F′: ctccagcacctgcagacatagctcagacagtacag; Frag2_R′: ttatctagatccggtggatctcactgccgtggcgcaag. All plasmids were sequence-verified to confirm they were error-free.

FRAP assay in living U2OS cells

FRAP experiments were performed using a Zeiss LSM880 confocal microscope at CO_2 and 37 °C with an oil immersion 63× objective lens (N.A. 1.4) and a Zen system (black edition). U2OS cells were co-transfected with eGFP-TDP-43 or eGFP-TDP-A315T along with mCherry-G3BP1. The oligomer/monomer/fibril were, respectively, treated with cells for 18 hours after 6 hours of transfection. After 18 hours of peptide treatments, FRAP experiments were performed as described above. For HSPi experiments, the cells were treated with HSPi (HSP70 inhibitor, VER-155008) and/or oligomers for 3 hours after 21 hours of transfection. For photobleaching the condensates, the green channel of the condensates was photobleached using a 405 nm laser at 50% power, and the red channel was carried out with a 561 nm laser at 100% power with 20 iterations, respectively. For each condition of photobleaching, at least 20 ROIs were carried out and analyzed. The relative fluorescence intensity of the photobleached region of interest (ROI) was determined by subtracting the mean intensity of the background from that of the photobleached ROI and then normalized to the mean intensity of the pre-bleached ROI.

Immunostaining

U2OS cells transfected or treated as indicated above were fixed with 4% paraformaldehyde, permeabilized with 0.1% NP-40, and pre-incubated with 5% BSA/PBS. For staining, primary antibodies were incubated overnight at 4 °C, followed by staining with secondary antibodies (1 : 1000 dilution) for 1 h. The dilution for primary antibodies is as follows: G3BP1 (Abcam, ab181150) was stained with 1 : 500 dilution, HSP70 (Proteintech, 10995-1-AP) with 1 : 1000 and pTDP-43 (pS409/410, Cosmo Bio, TIP-PTD-M01) with 1 : 500. Nuclei were stained with DAPI (1 : 10 000 dilution). Images were captured using a Zeiss LSM880 with 63× objective (N.A. 1.4) and the Zen system (black edition).

Author contributions

J. J. H., J. C. C., B. P. C. and C. C. L. conceived the project. B. P. C. designed and performed the oligomer extraction and characterization, including NMR spectroscopy, ThT fluorescence assay, turbidity measurement, LLPS analysis, and cell viability assay. C. C. L. designed and conducted the construct preparation, FRAP assay, fluorescence confocal microscopy, and immunostaining. R. Y. H. assisted with DIC microscopy. A. C. H. performed TEM imaging, dot blot analysis, and cell-free experiments. J. R. H. provided consultation on the TDP-CTD experiment and was responsible for protein purification. B. P. C. and C. C. L. wrote the manuscript. J. J. H. and J. C. C. revised the manuscript.

Conflicts of interest

The authors declare no competing financial interest.

Data availability

All data generated from this study are available upon request.

All experimental supporting data are available in the supplementary information (SI). Supplementary information: peptide sequence and additional data. See DOI: **https://doi.org/10.1039/d5sc05433h**.

Acknowledgements

We thank Dr Ruei-Yu He (Optical Microscopy Facility in Academia Sinica). We thank Guan-Wei Wu for supporting protein purification. We thank Dr Ya-Jen Cheng (Academia

Sinica Neuroscience Core Facility, AS-CF11-113-A6) for providing technical support in cell imaging. We thank Sue-Ping Lee, Shu-Mei Huang and Yae-Huei Liou from the Imaging Core of Institute of Molecular Biology, Academia Sinica for their support. We thank the mass spectrometry facility in the Institute of Chemistry, Academia Sinica.

References

1 T. Arai, M. Hasegawa, H. Akiyama, K. Ikeda, T. Nonaka, H. Mori, D. Mann, K. Tsuchiya, M. Yoshida, Y. Hashizume and T. Oda, TDP-43 is a component of ubiquitin-positive tau-negative inclusions in frontotemporal lobar degeneration and amyotrophic lateral sclerosis, *Biochem. Biophys. Res. Commun.*, 2006, **351**, 602–611.

2 B. S. Johnson, D. Snead, J. J. Lee, J. M. McCaffery, J. Shorter and A. D. Gitler, TDP-43 is intrinsically aggregation-prone, and amyotrophic lateral sclerosis-linked mutations accelerate aggregation and increase toxicity, *J. Biol. Chem.*, 2009, **284**, 25459.

3 E. L. Guenther, Q. Cao, H. Trinh, J. H. Lu, M. R. Sawaya, D. Cascio, D. R. Boyer, J. A. Rodriguez, M. P. Hughes and D. S. Eisenberg, Atomic structures of TDP-43 LCD segments and insights into reversible or pathogenic aggregation, *Nat. Struct. Mol. Biol.*, 2019, **26**, 988.

4 L. C. Koehler, Z. R. Grese, A. C. S. Bastos, L. D. Mamede, T. Heyduk and Y. M. Ayala, TDP-43 Oligomerization and Phase Separation Properties Are Necessary for Autoregulation, *Front. Neurosci.*, 2022, **16**, 818655.

5 E. S. Arnold, S. C. Ling, S. C. Huelga, C. Lagier-Tourenne, M. Polymenidou, D. Ditsworth, H. B. Kordasiewicz, M. McAlonis-Downes, O. Platoshyn, P. A. Parone, S. Da Cruz, K. M. Clutario, D. Swing, L. Tessarollo, M. Marsala, C. E. Shaw, G. W. Yeo and D. W. Cleveland, ALS-linked TDP-43 mutations produce aberrant RNA splicing and adult-onset motor neuron disease without aggregation or loss of nuclear TDP-43, *Proc. Natl. Acad. Sci. U. S. A.*, 2013, **110**, E736–E745.

6 Y. P. Sun, S. Q. Zhang, J. J. Hu, Y. Q. Tao, W. C. Xia, J. G. Gu, Y. C. Li, Q. Cao, D. Li and C. Liu, Molecular structure of an amyloid fibril formed by FUS low-complexity domain, *iScience*, 2022, **25**, 103701.

7 D. Arseni, R. R. Chen, A. G. Murzin, S. Y. Peak-Chew, H. J. Garringer, K. L. Newell, F. Kametani, A. C. Robinson, R. Vidal, B. Ghetti, M. Hasegawa and B. Ryskeldi-Falcon, TDP-43 forms amyloid filaments with a distinct fold in type A FTLD-TDP, *Nature*, 2023, **620**, 898–903.

8 C. Morelli, L. Faltova, U. C. Palmiero, K. Makasewicz, M. Papp, R. P. B. Jacquat, D. Pinotsi and P. Arosio, RNA modulates hnRNPA1A amyloid formation mediated by biomolecular condensates, *Nat. Chem.*, 2024, **16**, 1052–1061.

9 S. Wegmann, B. Eftekharzadeh, K. Tepper, K. M. Zoltowska, R. E. Bennett, S. Dujardin, P. R. Laskowski, D. MacKenzie, T. Kamath, C. Commins, C. Vanderburg, A. D. Roe, Z. Y. Fan, A. M. Molliex, A. Hernandez-Vega, D. Muller, A. A. Hyman, E. Mandelkow, J. P. Taylor and B. T. Hyman, Tau protein liquid-liquid phase separation can initiate tau aggregation, *EMBO J.*, 2018, **37**, e98049.

10 P. Arosio, T. P. J. Knowles and S. Linse, On the lag phase in amyloid fibril formation, *Phys. Chem. Chem. Phys.*, 2015, **17**, 7606–7618.

11 T. C. T. Michaels, A. Saric, S. Curk, K. Bernfur, P. Arosio, G. Meisl, A. J. Dear, S. I. A. Cohen, C. M. Dobson, M. Vendruscolo, S. Linse and T. P. J. Knowles, Dynamics of oligomer populations formed during the aggregation of Alzheimer's Aβ42 peptide, *Nat. Chem.*, 2020, **12**, 497.

12 M. Habashi, S. Vutla, K. Tripathi, S. Senapati, P. S. Chauhan, A. Haviv-Chesner, M. Richman, S. A. Mohand, V. Dumulon-Perreault, R. Mulamreddy, E. Okun, J. H. Chill, B. Guerin, W. D. Lubell and S. Rahimipour, Early diagnosis and treatment of Alzheimer's disease by targeting toxic soluble Abeta oligomers, *Proc. Natl. Acad. Sci. U. S. A.*, 2022, **119**, e2210766119.

13 Y. S. Fang, K. J. Tsai, Y. J. Chang, P. Kao, R. Woods, P. H. Kuo, C. C. Wu, J. Y. Liao, S. C. Chou, V. Lin, L. W. Jin, H. S. Yuan, I. H. Cheng, P. H. Tu and Y. R. Chen, Full-length TDP-43 forms toxic amyloid oligomers that are present in frontotemporal lobar dementia-TDP patients, *Nat. Commun.*, 2014, **5**, 4824.

14 M. S. Feiler, B. Strobel, A. Freischmidt, A. M. Helferich, J. Kappel, B. M. Brewer, D. Li, D. R. Thal, P. Walther, A. C. Ludolph, K. M. Danzer and J. H. Weishaupt, TDP-43 is intercellularly transmitted across axon terminals, *J. Cell Biol.*, 2015, **211**, 897–911.

15 X. B. Ding, Z. Xiang, C. Qin, Y. K. Chen, H. Y. Tian, L. Meng, D. H. Xia, H. Liu, J. Song, J. Fu, M. M. Ma and X. J. Wang, Spreading of TDP-43 pathology via pyramidal tract induces ALS-like phenotypes in TDP-43 transgenic mice, *Acta Neuropathol. Commun.*, 2021, **9**, 15.

16 W. M. Babinchak, R. Haider, B. K. Dumm, P. Sarkar, K. Surewicz, J. K. Choi and W. K. Surewicz, The role of liquid-liquid phase separation in aggregation of the TDP-43 low-complexity domain, *J. Biol. Chem.*, 2019, **294**, 6306–6317.

17 M. Hallegger, A. M. Chakrabarti, F. C. Y. Lee, B. L. Lee, A. G. Amalietti, H. M. Odeh, K. E. Copley, J. D. Rubien, B. Portz, K. Kuret, I. Huppertz, F. Rau, R. Patani, N. L. Fawzi, J. Shorter, N. M. Luscombe and J. Ule, TDP-43 condensation properties specify its RNA-binding and regulatory repertoire, *Cell*, 2021, **184**, 4680–4696.

18 F. Gasset-Rosa, S. Lu, H. Y. Yu, C. Chen, Z. Melamed, L. Guo, J. Shorter, S. Da Cruz and D. W. Cleveland, Cytoplasmic TDP-43 De-mixing Independent of Stress Granules Drives Inhibition of Nuclear Import, Loss of Nuclear TDP-43, and Cell Death, *Neuron*, 2019, **102**, 339–357.e337.

19 S. O. Shuster and J. C. Lee, Watching liquid droplets of TDP-43 age by Raman spectroscopy, *J. Biol. Chem.*, 2022, **298**, 101528.

20 L. Streit, T. Kuhn, T. Vomhof, V. Bopp, A. C. Ludolph, J. H. Weishaupt, J. C. M. Gebhardt, J. Michaelis and K. M. Danzer, Stress induced TDP-43 mobility loss independent of stress granules, *Nat. Commun.*, 2022, **13**, 5480.

21 J. E. Gu, C. Wang, R. R. Hu, Y. C. Li, S. N. Zhang, Y. P. Sun, Q. Q. Wang, D. Li, Y. S. Fang and C. Liu, Hsp70 chaperones TDP-43 in dynamic, liquid-like phase and prevents it from amyloid aggregation, *Cell Res.*, 2021, **31**, 1024–1027.

22 D. Mateju, T. M. Franzmann, A. Patel, A. Kopach, E. E. Boczek, S. Maharana, H. O. Lee, S. Carra, A. A. Hyman and S. Alberti, An aberrant phase transition of stress granules triggered by misfolded protein and prevented by chaperone function, *EMBO J.*, 2017, **36**, 1669–1687.

23 S. T. Kumar, S. Nazarov, S. Porta, N. Maharjan, U. Cendrowska, M. Kabani, F. Finamore, Y. Xu, V. M. Y. Lee and H. A. Lashuel, Seeding the aggregation of TDP-43 requires post-fibrillization proteolytic cleavage, *Nat. Neurosci.*, 2023, **26**, 983–996.

24 L. L. Jiang, J. Zhao, X. F. Yin, W. T. He, H. Yang, M. X. Che and H. Y. Hu, Two mutations G335D and Q343R within the amyloidogenic core region of TDP-43 influence its aggregation and inclusion formation, *Sci. Rep.*, 2016, **6**, 23928.

25 L. L. Jiang, M. X. Che, J. Zhao, C. J. Zhou, M. Y. Xie, H. Y. Li, J. H. He and H. Y. Hu, Structural Transformation of the Amyloidogenic Core Region of TDP-43 Protein Initiates Its Aggregation and Cytoplasmic Inclusion, *J. Biol. Chem.*, 2013, **288**, 19614–19624.

26 A. K. H. Chen, R. Y. Y. Lin, E. Z. J. Hsieh, P. H. Tu, R. P. Y. Chen, T. Y. Liao, W. L. Chen, C. H. Wang and J. J. T. Huang, Induction of Amyloid Fibrils by the C-Terminal Fragments of TDP-43 in Amyotrophic Lateral Sclerosis, *J. Am. Chem. Soc.*, 2010, **132**, 1186–1187.

27 G. C. H. Liu, B. P. W. Chen, N. T. J. Ye, C. H. Wang, W. L. Chen, H. M. Lee, S. I. Chan and J. J. T. Huang, Delineating the membrane-disrupting and seeding properties of the TDP-43 amyloidogenic core, *Chem. Commun.*, 2013, **49**, 11212–11214.

28 Y. L. Lin, Y. S. Cheng, C. I. Ho, Z. H. Guo, S. J. Huang, M. L. Org, A. Oss, A. Samoson and J. C. C. Chan, Preparation of fibril nuclei of beta-amyloid peptides in reverse micelles, *Chem. Commun.*, 2018, **54**, 10459–10462.

29 H. W. Chang, C. I. Yang and J. C. C. Chan, Incubation of Amyloidogenic Peptides in Reverse Micelles Allow Active Control of Oligomer Size and Study of Protein-Protein Interactions, *ChemMedChem*, 2024, **19**, e202400310.

30 S. Ray, T. O. Mason, L. Boyens-Thiele, A. Farzadfard, J. A. Larsen, R. K. Norrild, N. Jahnke and A. K. Buell, Mass photometric detection and quantification of nanoscale alpha-synuclein phase separation, *Nat. Chem.*, 2023, **15**, 1306–1316.

31 H. R. Li, W. C. Chiang, P. C. Chou, W. J. Wang and J. R. Huang, TAR DNA-binding protein 43 (TDP-43) liquid-liquid phase separation is mediated by just a few aromatic residues, *J. Biol. Chem.*, 2018, **293**, 6090–6098.

32 H. R. Li, T. C. Chen, C. L. Hsiao, L. Shi, C. Y. Chou and J. R. Huang, The physical forces mediating self-association and phase-separation in the C-terminal domain of TDP-43, *Biochim. Biophys. Acta, Proteins Proteomics*, 2018, **1866**, 214–223.

33 H. Sun, B. Yang, Q. Li, X. Zhu, E. Song, C. Liu, Y. Song and G. Jiang, Polystyrene nanoparticles trigger aberrant condensation of TDP-43 and amyotrophic lateral sclerosis-like symptoms, *Nat. Nanotechnol.*, 2024, **19**, 1354–1365.

34 F. Mori, H. Yasui, Y. Miki, T. Kon, A. Arai, H. Kurotaki, M. Tomiyama and K. Wakabayashi, Colocalization of TDP-43 and stress granules at the early stage of TDP-43 aggregation in amyotrophic lateral sclerosis, *Brain Pathol.*, 2024, **34**, e13215.

35 N. Fernandes, L. Nero, S. M. Lyons, P. Ivanov, T. M. Mittelmeier, T. A. Bolger and J. R. Buchan, Stress Granule Assembly Can Facilitate but Is Not Required for TDP-43 Cytoplasmic Aggregation, *Biomolecules*, 2021, **11**, 1367.

36 S. Lu, J. J. Hu, O. A. Arogundade, A. Goginashvili, S. Vazquez-Sanchez, J. K. Diedrich, J. G. Gu, J. Blum, S. Oung, Q. Z. Ye, H. Y. Yu, J. Ravits, C. Liu, J. Yates and D. W. Cleveland, Heat-shock chaperone HSPB1 regulates cytoplasmic TDP-43 phase separation and liquid-to-gel transition, *Nat. Cell Biol.*, 2022, **24**, 1378–1393.

37 A. F. Wang, X. Abulaiti, H. Zhang, H. Su, G. Z. Liu, S. R. Gao and L. S. Li, Cancer Cells Evade Stress-Induced Apoptosis by Promoting HSP70-Dependent Clearance of Stress Granules, *Cancers*, 2022, **14**, 4671.

38 Y. C. Li, J. G. Gu, C. Wang, J. J. Hu, S. Q. Zhang, C. Liu, S. N. Zhang, Y. S. Fang and D. Li, Hsp70 exhibits a liquid-liquid phase separation ability and chaperones condensed FUS against amyloid aggregation, *iScience*, 2022, **25**, 104356.

39 M. A. Gitcho, R. H. Baloh, S. Chakraverty, K. Mayo, J. B. Norton, D. Levitch, K. J. Hatanpaa, C. L. White, E. H. Bigio, R. Caselli, M. Baker, M. T. Al-Lozi, J. C. Morris, A. Pestronk, R. Rademakers, A. M. Goate and N. J. Cairns, A315T mutation in familial motor neuron disease, *Ann. Neurol.*, 2008, **63**, 535–538.

40 W. R. Guo, Y. B. Chen, X. H. Zhou, A. Kar, P. Ray, X. P. Chen, E. J. Rao, M. X. Yang, H. H. Ye, L. Zhu, J. H. Liu, M. Xu, Y. L. Yang, C. Wang, D. Zhang, E. H. Bigio, M. Mesulam, Y. Shen, Q. Xu, K. Fushimi and J. Y. Wu, An ALS-associated mutation affecting TDP-43 enhances protein aggregation, fibril formation and neurotoxicity, *Nat. Struct. Mol. Biol.*, 2011, **18**, 822–830.

41 M. Udan-Johns, R. Bengoechea, S. Bell, J. Y. Shao, M. I. Diamond, H. L. True, C. C. Weihl and R. H. Baloh, Prion-like nuclear aggregation of TDP-43 during heat shock is regulated by HSP40/70 chaperones, *Hum. Mol. Genet.*, 2014, **23**, 157–170.

42 Y. J. Chen and T. J. Cohen, Aggregation of the nucleic acid-binding protein TDP-43 occurs via distinct routes that are coordinated with stress granule formation, *J. Biol. Chem.*, 2019, **294**, 3696–3706.

43 U. Sengupta, A. N. Nilson and R. Kayed, The Role of Amyloid-β Oligomers in Toxicity, Propagation, and Immunotherapy, *Ebiomedicine*, 2016, **6**, 42–49.

44 C. T. Yeh, H. W. Chang, W. H. Hsu, S. J. Huang, M. H. Wu, L. H. Tu, M. C. Lee and J. C. C. Chan, Beta Amyloid Oligomers with Higher Cytotoxicity have Higher Sidechain Dynamics, *Chem.–Eur. J.*, 2023, **29**, e202301879.

45 H. W. Chang, H. Ma, Y. S. Wu, M. C. Lee, E. C. Y. Yuan, S. J. Huang, Y. S. Cheng, M. H. Wu, L. H. Tu and J. C. C. Chan, Site specific NMR characterization of abeta-40 oligomers cross seeded by abeta-42 oligomers, *Chem. Sci.*, 2022, **13**, 8526–8535.

46 T. O. Vogler, J. R. Wheeler, E. D. Nguyen, M. P. Hughes, K. A. Britson, E. Lester, B. Rao, N. Dalla Betta, O. N. Whitney, T. E. Ewachiw, E. Gomes, J. Shorter, T. E. Lloyd, D. S. Eisenberg, J. P. Taylor, A. M. Johnson, B. B. Olwin and R. Parker, TDP-43 and RNA form amyloid-like myo-granules in regenerating muscle, *Nature*, 2018, **563**, 508–513.

47 H. I. Ingolfsson, A. Rizuan, X. Liu, P. Mohanty, P. C. T. Souza, S. J. Marrink, M. T. Bowers, J. Mittal and J. Berry, Multiscale simulations reveal TDP-43 molecular-level interactions driving condensation, *Biophys. J.*, 2023, **122**, 4370–4381.

48 A. Molliex, J. Temirov, J. Lee, M. Coughlin, A. P. Kanagaraj, H. J. Kim, T. Mittag and J. P. Taylor, Phase separation by low complexity domains promotes stress granule assembly and drives pathological fibrillization, *Cell*, 2015, **163**, 123–133.

49 C. Wang, Y. J. Duan, G. Duan, Q. Q. Wang, K. Zhang, X. Deng, B. T. Qian, J. G. Gu, Z. W. Ma, S. Zhang, L. Guo, C. Liu and Y. S. Fang, Stress Induces Dynamic, Cytotoxicity-Antagonizing TDP-43 Nuclear Bodies via Paraspeckle LncRNA-Mediated Liquid-Liquid Phase Separation, *Mol. Cell*, 2020, **79**, 443–458.e447.

50 S. H. Johanna Ganssauge, S. Namboori, S.-K. Leung, J. Mill and A. Bhinge, Rapid and Inducible Mislocalization of Endogenous TDP43 in a Novel Human Model of Amyotrophic Lateral Sclerosis, *eLife*, 2024, **13**, RP95062.

51 G. M. Ginell and A. S. Holehouse, Hyperphosphorylation tunes TDP-43 solubility, *EMBO J.*, 2022, **41**, e111062.

52 P. H. Lin, G. W. Wu, Y. H. Lin, J. R. Huang, U. S. Jeng, W. M. Liu and J. R. Huang, TDP-43 Amyloid Fibril Formation via Phase Separation-Related and -Unrelated Pathways, *ACS Chem. Neurosci.*, 2024, **15**, 3767–3775.